J. Appl. Comput. Mech., 12(3) (2026) 1069-1083
DOI: 10.22055/jacm.2025.48746.5475

ISSN: 2383-4536
jacm.scu.ac.ir

Shahid Chamran University of Ahvaz

Journal of Applied and Computational Mechanics

Research Paper

Time-Dependent Reliability Analysis of Rotor-Blade Systems with Floquet-Moment-EVD Interval Approximation

Oscar Sanchez Jimenez, Emmanuel Pagnacco, Younes Aoues

INSA Rouen Normandie, Normandie Univ, LMN UR 3828, F-76000, Rouen, France,
Email: oscar.sanchez_jimenez@insa-rouen.fr (O.S.J.); emmanuel.pagnacco@insa-rouen.fr (E.P.); younes.aoues@insa-rouen.fr (Y.A)

Received September 12 2025; Revised December 04 2025; Accepted for publication December 15 2025.
✉ Corresponding author: O. Sanchez Jimenez (oscar.sanchez_jimenez@insa-rouen.fr)

Abstract. We study the time-dependent reliability problem of the linear time-periodic rotor-blade model under stochastic forcing, encompassing a broad class of mechanical systems (wind and tidal turbines, helicopter rotors). The periodic modes from Floquet theory are used to implement efficient moment-propagation convolution expressions for the response of the system, thus characterizing the limit state function. We then propose an interval-based decomposition strategy to estimate the probability of failure using results from Extreme Value Theory. The approach is compared with raw Monte Carlo simulation for a simplified rotor-blade structure subjected to Gaussian and non-Gaussian non-stationary loads, showing substantial gains in computation time and excellent accuracy. The approach is original and stands in contrast to instant-based discretization approaches popular in the time-dependent reliability literature.

Keywords: Rotor-blade models; Linear time-periodic systems; time-variant reliability; Extreme value theory; Floquet theory; non-Gaussian non-stationary stochastic process.

1. Introduction

Rotor–blade or bladed–disc models encompass a large family of machines and structures with broad scientific and industrial applications, describing such systems as wind and tidal turbines, helicopters, and other propulsion systems in maritime and aerospace devices. They emerge when the vibratory motion of continua (beams, bars, shells) is combined with traditional rotor–dynamics. The result is a system undergoing large rotations while simultaneously presenting the characteristics inherent to the vibration of beams, bars, or shells. A rich dynamical behavior emerges from the interactions of these two fields. At the same time, the underlying theory permits the analysis and design of systems that are present in many essential industries.

The emergence of rotor-blade models can be related to problems of rotating beams in the study of aerodynamic design [1, 2]; in the classical study of rotor-dynamics with finite elements [3, 4]; and in applied fields, such as helicopter control [5], to onshore [6] and offshore [7] tidal turbines. The modelling of blades as continua, as opposed to mere rigid bodies, is crucial for design and assessment, as highlighted in [8] for instance. Yet, such a modelling choice introduces a periodicity in the equations of motion of the system; periodicity can also be relevant when nonlinear effects are taken into account, and when periodic forcing is considered in elastic media [9]. In such cases, Floquet theory has proven effective in the stability analysis of these systems [5-9]. From a mathematical perspective, rotor–blade models can often be expressed in terms of systems of Ordinary Differential Equations (ODEs), with the particularity that the coefficient matrices are periodic on some parameter related to the system's angular velocity. These ODE systems with periodic coefficients are usually termed Linear time-periodic (LTP) systems [10]. They can be conceptualized as a generalization of traditional mechanical systems, the main difference being the periodicity of the coefficient matrices of system properties. Floquet theory ([11], a modern treatment can be found in [12]) is the theory of LTP ODEs. It has seen slow but increased application in the engineering domain.

Research efforts in rotor-blade systems, with and without the Floquet treatment, have centered on modelling, validation, and stability analysis [6, 7, 13-15]. There exists a gap in the study of the forced response of such systems. This gap is compounded by limited results in the consideration of uncertainties or stochasticity for these models, exceptions including the works [16-18], which focus, however, on parameter uncertainty and not input uncertainty. This poses limitations for the adoption of the reliability framework in rotor-blade systems. The modeling of system uncertainty and stochastic loads within the rotor–blade LTP framework poses important conceptual and technical challenges. The stochastic response of this type of system is generally non-stationary [19], increasing the computational burden in memory and time of even simple analysis tools. Similarly, the stochastic load is often non–Gaussian, limiting the applicability of many classical results. Nevertheless, some efforts in this sense include works such as [20, 21], and more recently [22].

Published online: December 21 2025

Reliability analysis concerns the study of the probability of failure in components and systems. This approach has been widely adopted in engineering practice over the last 30 years, enabling the integration of uncertainties in both structures and external loads. Among the remaining challenges in the study of reliability, the investigation of time-dependent Limit State Functions (LSFs) has garnered significant interest over the past 30 years. Such problems arise in the presence of non-stationary load processes over structures and machines, as well as when degradation mechanisms are considered in the system's model. The advantage of such choices is the possibility of describing realistic and complex engineering situations with higher precision. As remarked in [23], time-dependent problems stand as the main challenge in the field, along with LSFs that are expensive to evaluate from a computational perspective. Time-dependence introduces a significant challenge to traditional, well-established methods for time-independent reliability. A review of the developments of time-variant reliability is presented in [24], giving a global perspective of the subject.

Significant works in time-dependent reliability follow the general framework proposed in [25]; the now-classical methods for TVR PHI2 [26] and PHI2+ [27]; more recent developments include JUR/FORM [28], m-EGO [29], and NEWREL [30]. The main idea in these methods is to introduce a temporal discretization of the LSF. From another perspective, a vibrant area of research known as Active–Learning Reliability (ARL), pioneered by works such as [31], in which Monte-Carlo simulation (MCS) is combined with Kriging in a method that updates the surrogate models with relevant training points near the crossing of the LSF until a certain convergence or precision criteria is met. The EVD-based TVR proposal in [32] builds upon a similar Active Learning strategy and Kriging surrogate models, resulting in an efficient TVR method of a general nature.

There are two main challenges in applying these methods to the study of rotor-blade models. First, classic methods such as PHI2 or JUR/FORM are not adapted for response processes resulting from a stochastic dynamic problem. In these frameworks, the LSF is reformulated from previous analysis to be expressed in input-output terms, thus decoupling the LSF from the underlying dynamical problem. Second, ARL techniques, including m-EGO [29] and AK-MCS [31] are general approaches that treat the LSF as black boxes, neglecting the problem-specific structure. They also require substantial technical machinery (from experimental design to surrogate model selection and implementation) to arrive at the target solution. Some results exist in the time-dependent reliability of tidal and hydrokinetic turbine blades, such as [33, 34]. These works propose complex FEA models to simulate the blades but neglect the treatment of the system as a rotor-blade model; the system is often analyzed in static conditions [33], simplify the stochastic input to stationary gaussian processes [34]. This is a result of the steep computational cost of running such computational models, and these compromises are understandable.

We propose a model-specific time-dependent reliability framework for rotor-blade models under stochastic loading. Our method exploits the mathematical structure of LTP dynamics using Floquet theory and efficient uncertainty propagation semi-analytical convolution equations to quantify the moments of the system's response. Then, we introduce an interval decomposition algorithm to identify "important intervals" in the response based on the associated LSF, finally constructing an EVD-based interval approximation of the failure probability. Our method is adapted to stochastic dynamics problems; it is effective for Gaussian and non-Gaussian inputs and can handle stationary and non-stationary inputs alike. From a technical perspective, it is economical, as it relies on simple convolutions for moment propagation, a straightforward moment analysis procedure, and a simple EVD approximation based on relatively simple assumptions. Our method:

- Has very good accuracy compared to the MCS benchmark;
- Enables the use of simple EVD theory and Poisson's hypothesis;
- Significantly reduces computation time, even when compared to an optimized parallel MCS benchmark;
- Has practical application to real engineering problems.

The organization of this paper is as follows: Section 2 offers a summary of the relevant background developments, from rotor–blade models and their LTP representation, to key findings from Floquet theory and the basic formulations of stochastic modelling and time-variant reliability; Section 3 introduces the first element of our proposal, the moment–propagation formulation harnessing Floquet modal forms to obtain convolution equations to quantify the LSF; in Section 4, Extreme Value Theory is used as the basis for the second element of our proposal, the interval analysis of propagated moments to approximate the LSF and the probability of failure of the system; Section 5 presents a numerical application testing our proposal, with discussion about technical aspects and results; finally, the conclusion summarizes our developments and our main findings.

2. Theoretical Background

This section provides the essential theoretical background for our development. First, rotor-blade models are briefly described, presenting their corresponding LTP equations of motion. Second, the relevant results from Floquet theory are summarized. Finally, we introduce basic notions related to stochastic processes and reliability, to fixate notation and the conventions to be followed throughout our development.

2.1. Rotor-blade LTP models

A rotor–blade model, also known as a bladed–disc model, emerges when a rotor system is augmented with blade elements, which are described as elastic elements. The blades can be modeled as beams, describing the transverse vibration of these elements and their effect on the underlying rotor. This type of model displays many of the features found in standard rotor dynamics (modal dependence on the angular velocity, gyroscopic effects, ...), with the added difficulty of the elastic deformation of the blade, which translates into an evolution of the inertial properties of the rotor with time.

In Fig. 1, we present the schematic configuration of a rotor-blade system. Our modelling and general treatment is presented in Appendix A. Detailed expositions of the underlying rotor dynamics are provided in [35, 36]. Suppose small angular motion is assumed and the translation in the direction of the shaft's longitudinal axis (normal to the page) is negligible. In such a case, the 5–DOF rotor model can be simplified to a 2–DOF planar motion rotor system, describing the dynamics of the system in Fig. 1. From this simplification, we represent, in Fig. A1, the equivalent representation of the rotor–support–mast element: the elastic and damping properties of the support can be reduced into a rotor-spring-damper system with translations constrained to the plane of rotation.

The blades, modeled here as Euler–Bernoulli beams approximating the properties of those shown in Fig. 1. Their transverse vibration can be approximated by means of kinematic discretization and modal approximation (see Appendix A). From the Euler-Bernoulli rotating beam problem, one can approximate the mode shapes of the beam onto a polynomial basis truncated at the desired number of modes. This approach is presented in [37] for a traditional Euler–Bernoulli beam, but it can be extended to solve the rotating Euler-Bernoulli beam (see [19]). This modal approximation facilitates the formulation of the assembled system, using a common kinematic description to formulate the kinetic and potential energies, from which a total Lagrangian can be computed and the Euler–Lagrange equations can be used to obtain the equations of motion of the rotor–blade assembly.

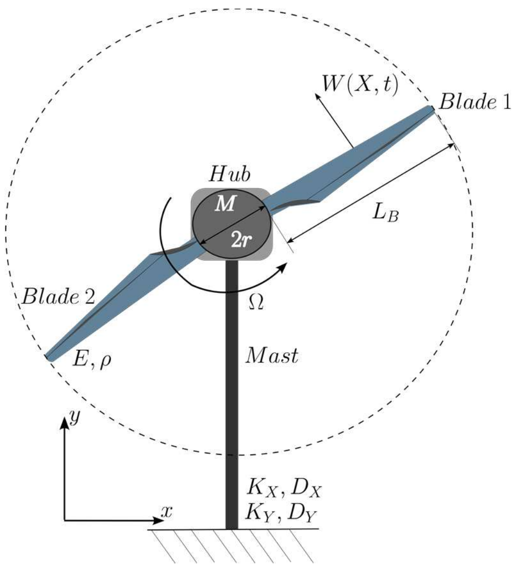

Fig. 1. Schematic representation of planar rotor-blade system with main physical and kinematic features; the values of represented quantities are provided in Tables 2 and 3.

Finally, Fig. 1, the external agent acts on the system normal to the plane, inducing a load normal to the blade's axis. If fluid–structure interactions are considered, one may consider an incident velocity field acting on the rotor and its blades. Notice that even if the acting velocity field is supposed to be uniform, the rotation of the system will result in inherently oscillatory forces. For brevity, we only present the general form of the equations of motion for the 6–DOF rotor–blade system that will be the subject of our study, their details are reported in Appendix A. More detailed models can be found in [5, 19]. The equation of motion has the following standard form:

$$\mathbf{M}(t)\ddot{\mathbf{x}} + \mathbf{G}_t(t)\dot{\mathbf{x}} + \mathbf{K}_t\mathbf{x} = \mathbf{f}(t) \tag{1}$$

Here $\mathbf{x} = [x_1, \ldots, x_6]$, dot notation represents a derivative with respect to time. The first two DOFs correspond to horizontal and vertical translation of the geometric center of the rotor, respectively. DOFs 3 and 4 represent the modal coordinates of beam 1, and similarly, DOFs 5 and 6 represent the modal coordinates of the second beam. The time-dependent matrices verify: $\mathbf{M}(t+T_p) = \mathbf{M}(t)$; $\mathbf{G}_t(t+T_p) = \mathbf{G}_t(t)$, for the period of the system T_p. The previous equation can be cast into state space form:

$$\dot{\mathbf{y}} = \mathbf{A}(t)\mathbf{y} + \mathbf{B}(t)\mathbf{f}(t) \tag{2}$$

These new matrices, $\mathbf{A}(t), \mathbf{B}(t)$ have the same period T_p, which makes them suitable for the application of Floquet analysis. The structure of these matrices is provided in Appendix A. Finally, one can define a convenient matrix **C** that facilitates the computation of quantities of interest computed from the response (See Appendix A for more details):

$$S(t) = \mathbf{C}\mathbf{y}. \tag{3}$$

2.2. Floquet theory

The central result of Floquet theory concerns the existence of a transformation of Eq. (1), of the form:

$$\mathbf{y} = \mathbf{R}(t)\mathbf{q}. \tag{4}$$

Here, $\mathbf{R}(t)$ is a matrix containing the Right periodic eigenvectors of the system, and **q** are new modal variables. Defining the Left Periodic Eigenvectors as $\mathbf{L}(t) = \mathbf{R}^{-1}(t)$, Eq. (2) can be transformed to [10]:

$$\dot{\mathbf{q}} = \rho\mathbf{q} + \mathbf{L}(t)\mathbf{B}(t)\mathbf{f}(t) \tag{5}$$

The homogeneous part of this equation is time-invariant and decoupled, ρ is a constant diagonal matrix in the non-degenerate case, containing the Characteristic Exponents of the system [12]. The Impulse Response Function of this system is $\mathbf{h}(t) = \exp[\rho t]$ [10], from which the forced response of the system can be obtained:

$$\mathbf{y}_f(t) = \mathbf{R}(t)\int_0^t \mathbf{h}(t-\tau)\mathbf{L}(\tau)\mathbf{B}(\tau)\mathbf{f}(\tau)d\tau. \tag{6}$$

This last expression will serve as the basis for our moment propagation strategy in Section 3.

2.3. Stochastic processes

We consider a stochastic process $S(t)$, which is an ensemble of random variables indexed by the continuous parameter t. The complete characterization of this process, in all generality, is given by its finite-dimensional joint density distributions. For applications, notably in probabilistic mechanics, it is practical to assume processes with sufficient regularity as to be described by their first few moments, or equivalently, their first few joint densities. We may write the generic n-dimensional joint Cumulative Distribution Function (CDF) as:

$$P_{S\ldots S}(s_1, \ldots, s_n; t_1, \ldots, t_n) = \mathbb{P}[S(t_1) \le s_1, \ldots, S(t_n) \le s_n] \tag{7}$$

Denoting the mathematical expectation by $\mathrm{E}[\bullet]$, we can define the mean function of S(t) as:

$$\mu_S(t) = \mathrm{E}[S(t)]. \tag{8}$$

The covariance function is defined as:

$$\Sigma_{SS}(t_1,t_2) = \mathrm{E}\left[\left(S(t_1) - \mu_S(t_1)\right)\left(S(t_2) - \mu_S(t_2)\right)\right], \tag{9}$$

with the variance function given by $\sigma_{SS}(t) = \Sigma_{SS}(t,t)$. Under suitable continuity conditions on the covariance function, the covariance of the derivative process can be obtained by differentiation: $\Sigma_{\dot{S}S}(t_1,t_2) = \frac{\partial}{\partial t_1}\Sigma_{SS}(t_1,t_2)$; $\Sigma_{\dot{S}\dot{S}}(t_1,t_2) = \frac{\partial}{\partial t_1}\frac{\partial}{\partial t_2}\Sigma_{SS}(t_1,t_2)$.

2.4. Extreme value distribution and reliability

The Extreme Value of a stochastic process S(t) in $0 \le t \le T$ is the following random variable:

$$S_M = \mathrm{Max}_{[0,T]}[S(t)]. \tag{10}$$

Its connection to the reliability or the probability of failure is easily established, considering the following type of time-dependent LSF:

$$G(t) = L - S(t) \tag{11}$$

where *L* is a constant and deterministic available resistance. The failure criterion here is delimited by $G(t) \le 0$, and the probability of failure over the entire interval $0 \le t \le T$, denoted by P_f^C, can be obtained from:

$$P_f^C = \mathbb{P}[G(t) \le 0, \exists t \in [0,T]]. \tag{12}$$

The probability of crossing into the unsafe domain can be expressed in terms of the EVD of S(t):

$$P_S = P_{S_M}(L) \tag{13}$$

where $P_{S_M}(L) = \mathbb{P}[S_M \le L]$ is the CDF of the random variable S_M evaluated at *L*; it represents the probability that the maximum of process S(t) in $0 \le t \le T$ is at most *L*, and P_S is the reliability of the system, which is the probability of non-failure. The probability of failure P_f^C is the conjugate, in the probability sense, of the reliability:

$$P_f^C = 1 - P_S = 1 - P_{S_M}(L) \tag{14}$$

A popular approach to computing the EVD of a process relies on the study of the crossing intensity or crossing rate $\nu_S^+(t)$ of said process. Rice established a central result with the so–called Rice formula approach (see [38-40] for a modern exposition). More recent developments include [41]; from an applications perspective: [42] in random vibrations, [43] in stochastic mechanics and simulation, [44] in applied multivariate processes. Our exposition here is limited to the pertinent results, acknowledging the vast literature around this problem since the works of Rice.

The crossing rate (also crossing intensity or upcrossing rate) can be obtained from the Rice formula [40]:

$$\nu_S^+(t)dt = dt\int_{-\infty}^{+\infty} |z| p_{S\dot{S}}(0,z,t)dt \tag{15}$$

Here, $p_{S\dot{S}}$ is the joint Probability Density Function (PDF) of the stochastic process $S(t)$ and its derivative $\dot{S}(t)$. The limitation of this formula is the difficulty in evaluating the corresponding integral for general distributions, and the lack of information to compute the PDF when the response process is not fully characterized, as often, only a few moments or a few realizations of the process are available. Two quantities of interest associated to $\nu_S^+(t)$: the number of crossings of $S(t)$ over the threshold *L* on $[0,T]$, $N(L,0,T)$; and the mean number of crossings of $S(t)$ over the threshold *L* on $[0,T]$, $\lambda_S^+(L)$. Expressions for these quantities are [42, 44]:

$$\begin{gathered} \mathrm{E}[N(L,0,T)] = \int_0^T \nu_S^+(t,L)dt \\ \lambda_S^+(L) = \mathrm{E}[N(L,0,T)] \end{gathered} \tag{16}$$

Finally, we will add that analytical solutions exist for several types of Gaussian processes, including the univariate stationary case, the multivariate stationary case, and some versions of the non-stationary case. For instance, for the univariate stationary Gaussian case, we have:

$$\nu_S^+(t) = \frac{1}{2\pi}\sqrt{\frac{\sigma_{\dot{S}\dot{S}}}{\sigma_{SS}}}\exp\left[-\frac{(L-\mu_S)^2}{2\sigma_{SS}}\right]. \tag{17}$$

However, the applicability of the expressions for general non-stationary processes is limited, notably because in many situations they suffer from numerical instabilities when oscillatory moments are involved, and these take values close to or crossing zero.

Bridging the gap between $\nu_S^+(t)$ and the EVD is the Poisson hypothesis, which yields the following expression:

$$P_{S_M}(L) = P_S(L;t=0)\exp[\lambda_S^+(L)]. \tag{18}$$

Note that the Poisson hypothesis assumes:

- Threshold crossings are rare events;
- Successive crossings are statistically independent;
- The crossing intensity of the rate of upcrossing is constant over the observation interval.

But for LTP systems:

- Periodicity of response moments leads to correlations between crossings;
- The crossing intensity of the rate of upcrossing varies with the periodicity of the system;
- If applied, EVD approximations may misrepresent the actual failure probability.

Our proposal tries to address some of these limitations. In particular, while we still use a Poisson-like EVD, it is now constructed from an approximation on critical intervals and at constant crossing rate; the rest of the instants in the observed process are excluded from the analysis. While this approximation incurs in an error, this error is reducible, as we will illustrate. On the other hand, by removing these instants from the analysis, we overcome the breakdown resulting from trying to apply Poisson to the entire response process.

3. Moment Propagation by Floquet Modal Convolution

We now consider Eq. (6) with a multivariate stochastic input $\mathbf{f}(t)$, with known moments. We highlight the fact that all processes generalizing deterministic quantities from Section 2.2 retain their dimension, so they are multivariate stochastic processes. Consequently, the associated moments are vectors in the case of the mean function and matrices in the case of the covariance function. The observation matrix transforms the response into a scalar response $S(t)$.

We seek to determine the quantity of interest $S(t)$ from the forced response $\mathbf{y}_f(t)$, although throughout our development, we will simply note it by $\mathbf{y}(t)$, ignoring the homogeneous response. This is justified since the homogeneous response decays in damped systems, leaving only the forced component to study the long-term behavior.

We first introduce the adapted load $\mathbf{p}(t)=\mathbf{L}(t)\mathbf{B}(t)\mathbf{f}(t)$, combining the physical load with the periodic system matrix $\mathbf{B}(t)$ and the generally complex Left Periodic eigenvector matrix $\mathbf{L}(t)$. This is done for notational convenience. Applying the expectation on both sides of Eq. (6), we obtain:

$$\begin{aligned}
\mathrm{E}[\mathbf{y}(t)] &= \mathrm{E}\left[\mathbf{R}(t)\int_0^t \mathbf{h}(t-\tau)\mathbf{p}(\tau)d\tau\right] \\
\boldsymbol{\mu}_y(t) &= \mathbf{R}(t)\int_0^t \mathbf{h}(t-\tau)\mathrm{E}[\mathbf{p}(\tau)]d\tau \\
\boldsymbol{\mu}_y(t) &= \mathbf{R}(t)\int_0^t \mathbf{h}(t-\tau)\boldsymbol{\mu}_p(\tau)d\tau
\end{aligned} \tag{19}$$

Applying Eq. (3):

$$\mu_S(t)=\mathbf{CR}(t)\int_0^t \mathbf{h}(t-\tau)\boldsymbol{\mu}_p(t)d\tau. \tag{20}$$

A similar procedure can be applied to compute any desired moment. In this work, we will limit the scope to the second moment centered around the mean, the covariance function. We have, with $\tilde{\mathbf{p}}(t)=\mathbf{p}(t)-\boldsymbol{\mu}_p(t)$:

$$\begin{aligned}
\mathrm{E}\left[\left(\mathbf{y}(t_1)-\boldsymbol{\mu}_y(t_1)\right)\left(\mathbf{y}(t_1)-\boldsymbol{\mu}_y(t_1)\right)^H\right] &= \mathrm{E}\left[\left(\mathbf{R}(t_1)\int_0^{t_1}\mathbf{h}(t_1-\tau_1)\tilde{\mathbf{p}}(\tau_1)d\tau_1\right)\left(\mathbf{R}(t_1)\int_0^{t_2}\mathbf{h}(t_2-\tau_2)\tilde{\mathbf{p}}(\tau_2)d\tau_2\right)^H\right] \\
\boldsymbol{\Sigma}_{yy}(t_1,t_2) &= \mathbf{R}(t_1)\int_0^{t_2}\int_0^{t_1}\mathbf{h}(t_1-\tau_1)\mathrm{E}\left[\tilde{\mathbf{p}}(\tau_1)\tilde{\mathbf{p}}^H(\tau_2)\right]\mathbf{h}^H(t_2-\tau_2)d\tau_1 d\tau_2\mathbf{R}^H(t_2) \\
\boldsymbol{\Sigma}_{yy}(t_1,t_2) &= \mathbf{R}(t_1)\int_0^{t_2}\int_0^{t_1}\mathbf{h}(t_1-\tau_1)\boldsymbol{\Sigma}_{pp}(\tau_1,\tau_2)\mathbf{h}^H(t_2-\tau_2)d\tau_1 d\tau_2\mathbf{R}^H(t_2)
\end{aligned} \tag{21}$$

Here, the superscript H denotes the complex conjugate, and its necessity comes from the fact that $\mathbf{p}(t)$ is a complex stochastic process. Now Eq. (21) can be combined with Eq. (3) to yield:

$$\Sigma_{SS}(t_1,t_2)=\mathbf{CR}(t_1)\int_0^{t_2}\int_0^{t_1}\mathbf{h}(t_1-\tau_1)\mathrm{E}\left[\tilde{\mathbf{p}}(\tau_1)\tilde{\mathbf{p}}^H(\tau_2)\right]\mathbf{h}^H(t_2-\tau_2)d\tau_1 d\tau_2\mathbf{R}^H(t_2)\mathbf{C}^H \tag{22}$$

From the covariance function, the variance function of $S(t)$ can be obtained, as previously shown. Similarly, $\Sigma_{SS}(t_1,t_2)$ can be differentiated to obtain $\Sigma_{\dot{S}S}(t_1,t_2)$ and $\Sigma_{\dot{S}\dot{S}}(t_1,t_2)$, and their respective variances. This can be done numerically, which is the approach we take here.

This development shows that, in the general case, the stochastic response of this type of system is nonstationary even when the load is stationary, given the time-modulation of the periodic modes. The Limit State Function (LSF) derived from the stochastic response will be itself a nonstationary process, which frames the problem within the domain of TVR.

4. Time-Variant Reliability Estimation by Interval Decomposition and Extreme Value Theory

4.1. Motivation of interval decomposition

The inspiration for our approach is motivated by the remarkable result in [45]. In this article, the EVD of a cyclostationary Gaussian process is obtained. A cyclostationary Gaussian process is one with a periodic covariance function on its time arguments. Under reasonable regularity assumptions on the Gaussian cyclostationary process:

1. The EVD can be expressed, asymptotically, by considering the maximal variance on a single period;
2. If over a single period, the variance is maximal over finitely many points (of time), a sum of the asymptotic EVDs at points of maximal variance yields the total EVD;
3. If the cyclostationary process is observed in an interval with multiple periods, again, the total EVD can be expressed as the sum of the EVDs of each period.

The results from Konstant and Piterbarg, while insightful, have certain limitations for our application:

- First, the results are asymptotic; in our terminology, they apply only to arbitrarily large 'deviations' or l. This means their EVD distribution is not applicable to our study;
- Second, cyclostationarity is a relatively strong condition, with many systems approaching but not fully verifying it;
- Third, their results are established for centered (zero mean) processes.

We retain the idea of decomposing the variance of the non-stationary process into intervals with a single maximum to add the EVDs from each interval then. However, we have to adapt the idea to the non-centered case in which the mean function is also time-variant, and we have to replace the asymptotic EVD distribution by a more feasible one (in our case, the Poisson hypothesis is made). Our method is heuristic in nature and decomposes the mean and variance functions into intervals. Then, the peak mean and peak variance are identified, and based on their relation, certain unimportant intervals are excluded. Next, peak mean and variance values are used, along with an equivalent sub-interval length, to compute the EVD of each interval. Finally, the total EVD is calculated as the sum of the EVDs from each interval.

4.2. Interval decomposition idea

We seek to construct a reliability estimation based on an EVD approximation of the form (from Eq. (14) and Eq. (18)):

$$\begin{aligned} P_f^C &= 1 - P_{S_M}(L) \\ &\approx 1 - \exp\left[\hat{\lambda}_S^+(L)\right] \end{aligned} \tag{23}$$

where $\exp[\hat{\lambda}_S^+(L)]$ is a sum of EVDs in Poisson form, of contributions:

$$\hat{\lambda}_S^+(L) = \sum_k \Delta t_k \hat{v}_{S,k}^+ \tag{24}$$

for k contributions of importance. In this expression, Δt_k is some small interval of time over which $\hat{v}_{S,k}^+$ can be considered as approximately constant, and $\hat{v}_{S,k}^+$ is one of the k crossing rates associated with peak variance events in the time-varying variance function. Throughout our developments here, we invite the reader to analyze the associated graphic representation provided in Fig. 2 for illustrative purposes.

We make the following basic observations:

1. The moments of S(t) are periodic or approximately periodic, but do not necessarily share the same minimal period;
2. For elevated thresholds L, important contributions to the probability of crossing require high values of $\mu_S(t)$;
3. Important contributions to the probability of crossing are associated with peak variance events.

From these observations, it becomes apparent that we need to analyze the mean and variance functions of S(t) to identify intervals with meaningful contributions to crossings, or equivalently, to the probability of failure. These contributions must verify a high level of the mean and the variance, not just peak variance. To identify these contributions, we introduce a hierarchical interval sieve, where we will introduce several interval decompositions of the quantities involved, selecting the ones of importance.

In this hierarchy, we begin with level zeroth, $I^T = [t_0, T]$, encompassing the entire observation time of the process S(t). We select subintervals of I^T in which the mean function maintains high values, generating level 1 $I^{(1)} = \bigcup_k I_k^{(1)}$. For each subinterval $I_k^{(1)} = [t_{0,k}, T_k]$, and it contains as many "high mean" intervals as can be identified on I^T. To quantify the "high values" of the mean function $\mu_S(t)$, we use the temporal average of $\mu_S(t)$ over I^T:

$$\xi = \frac{1}{T - t_0} \int_{t_0}^{T} \mu_S(t)\,dt \tag{25}$$

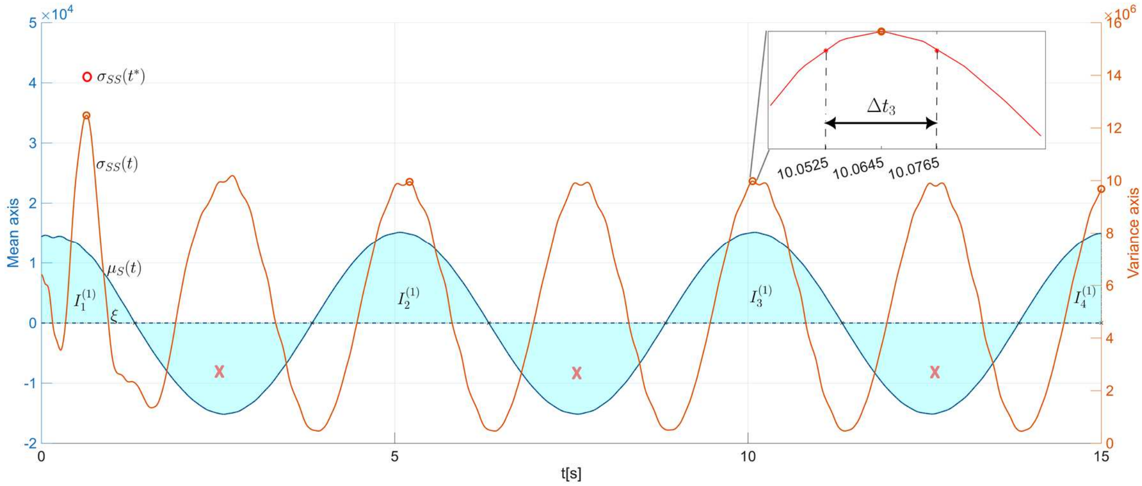

Fig. 2. Graphical representation of the interval decomposition idea, displaying the mean (left axis) and the variance (right axis) function with a common time axis. The pertinent maxima of the variance are highlighted. The temporal average of the mean and its intersections with the mean function are shown, and the intervals defined by the intersection are shaded in blue. The entire time axis represents the level zeroth interval; intervals of level 1 are labeled. A zoom of the third interval of level 1 is included, illustrating the peak variance and the associated level 2 interval.

So that pairs of instants verifying $\mu_S(t)-\xi=0$ split I^T into intervals where $\mu_S(t)$ is above and below ξ, respectively. We retain only the intervals in which $\mu_S(t)>\xi$ to form $I_k^{(1)}$. Notice that I^T is a single interval, whereas $I^{(1)}$ is a family of subintervals.

The next step is finding the maximal variance for each subinterval in $I^{(1)}$. From this step, peaks in variance that coincide with low (or even negative) values of the mean are systematically excluded from the analysis, as desired. In our study, we limit the complexity of this step to a single peak in variance per subinterval, although further research in this direction is envisioned.

The final level in our hierarchy consists of the subintervals that define Δt_k. We define these subintervals by statistical similarity between points of maximal variance and their immediate neighborhood. We define the following normalized covariance:

$$\Upsilon_{SS}\left(t^*,t\right)=\frac{\Sigma_{SS}\left(t^*,t\right)}{\mathrm{Max}\left[\Sigma_{SS}\left(t^*,t\right)\right]}, \tag{26}$$

where the argument t^* is fixed, for each subinterval of $I^{(1)}$ it is defined as $t^*=\mathrm{ArgMax}[\sigma_{SS}(t)],\ t\in I_k^{(1)}$. Now, $0\le\Upsilon_{SS}\le 1$, with 1 being verified by $t=t^*$. To construct the second and final level of intervals $I_k^{(2)}=\bigcup_k I_k^{(2)}$, for each element of $I^{(1)}$ we search for $\theta_{k,0},\theta_k\in I_k^{(1)}$ such that $\Upsilon_{SS}(t^*,\theta_{k,0})=\Upsilon_{SS}(t^*,\theta_k)=\beta$, and $I_k^{(2)}=[\theta_{k,0},\theta_k]$. Then, $\Delta t_k=\theta_k-\theta_{k,0}$.

The parameter β is important, since it determines the size of the final subintervals which are used in the approximation. More precisely, it sets the width of the temporal interval over which we approximate the crossing rate as constant, with maximal mean and variance. It is what allows the passage from asymptotic expressions, where crossings happen at points, to more realistic scenarios with finite thresholds. In Eq. (26), and from the previously established conditions, we see that this parameter defines a small vicinity around the instant of peak variance, which are so probabilistically correlated that approximating them as a single event is a reasonable approximation.

If we let $\beta\to 0$, then the approximation fails because the interval is too broad: all points in the above-mean subinterval are approximated as having peak variance, which greatly overestimates the probability of failure. On the other hand, if we let $\beta\to 1$, the interval collapses into a point, and the asymptotic case is recovered, but the interval approximation is no longer valid because the probability of failure will be zero: we have zero width interval. This parameter should be sufficiently small so that all important instants around peak variance are accounted for in the approximation, yet large enough as not to collapse into a singular point or leave regions with meaningful likelihood of crossing excluded from the approximation. What is needed is a criterion to identify instants sufficiently correlated with the response process at $S(t^*)$.

We propose a criterion based on the covariance function around t^*. We start with the covariance function around t^* for the corresponding $I_k^{(1)}$ interval:

$$\Sigma(\beta)=\begin{bmatrix}\Sigma_{SS}\left(t^*,t^*\right) & \Sigma_{SS}\left(t^*,t_\beta\right)\\ \Sigma_{SS}\left(t_\beta,t^*\right) & \Sigma_{SS}\left(t_\beta,t_\beta\right)\end{bmatrix} \tag{27}$$

where $t_\beta=\theta_k$ for a given (variable) β. This discretized covariance provides a measure of the correlation between the response process at peak variance time and the time at the end of the interval generated by the chosen β, such measure is quantified with its determinant:

$$Z(\beta)=\mathrm{Det}\left[\Sigma(\beta)\right] \tag{28}$$

This determinant increases as β approaches one, since t_β is closer to peak variance; however, after a certain threshold, this determinant begins to decrease, eventually becoming zero: this effect expresses the fact that the instants have become indistinguishable and the covariance becomes singular. We select β as a value right before this inflection point takes place: this means the instants are sufficiently correlated to make our approximation meaningful, but also guarantees that the approximation is sufficiently far from the onset of singularities, or that important points are being excluded. This choice of parameter implies an analysis of the covariance function of the response, which is readily available from the moment convolution; it incurs in a negligible additional computation time. In Appendix B, we provide visualizations of this type of analysis.

For the final intervals we may compute the following moments:

$$\mu_S^{\max,i}=\mathrm{Max}_{I_i^{(1)}}\left[\mu_S\left(t\right)\right];\quad \sigma_{SS}^{\max,i}=\mathrm{Max}_{I_i^{(1)}}\left[\sigma_S\left(t\right)\right];\quad \sigma_{\dot S\dot S}^{\max,i}=\sigma_{\dot S\dot S}\left(t^*\right);\quad \forall i\in k. \tag{29}$$

With these moments, $\hat{\nu}_{S,k}^{+}(t)$ can be computed for each interval of importance, using, for instance, Eq. (17) as a local Gaussian stationary approximation. At this stage, some comments about the method's behavior are in place. First, when β is selected according to our proposed criterion, and the EVD approximation is based on the moments specified in Eq. (29), we are always overestimating the EVD and thus the probability of failure. This is because we are approximating each interval $I_k^{(2)}$ with the maximum mean and variance of this interval, where we can see from the schematic representation in Fig. 2 that this is not strictly so. If the parameter β is selected after the inflection point described in this section and in Appendix B, we would then be leaving out of the approximation important instants in which crossings are likely to happen, leading to underestimation of the EVD. As will be shown in our numerical results, this overestimation guarantee holds for our case studies, and it can be made very small if the right β is selected, by a judicious covariance analysis.

Our developments in this section and Section 3 can be combined into complementary subprocedures. In Fig. 3, we present the general algorithmic implementation and integration of our method. Table 1 provides a summary of our interval hierarchy.

Table 1. Summary of interval hierarchy.

Class	Description	Meaning
Level zeroth, I^T	Total time interval	Initial and final time
Level one, $I^{(1)}$	Set of subintervals	Above-mean intervals
Level two, $I^{(2)}$	Set of subintervals	Critical intervals

Table 2. Physical parameters of the rotor component in the rotor-blade application.

Disc mass (M)	Disc diameter (2r)	Base springs (K_X, K_Y)		Base damping (D_X, D_Y)	
1000.0 [kg]	2.0000 [m]	2.0000×10^6	5.0000×10^8 [N.m^{-1}]	30.000	20.000 [N.s.m^{-1}]

Function 1 Floquet–Moment–EVD Interval approximation algorithm

Input: $\mathbf{A}(t)$, $\mathbf{B}(t)$, T_p, $[t_0, t_f]$, $\mathbf{f}(t)$, L
Output: $\hat{P}_f^c$
1: **procedure** FLOQUET–MOMENT–EVD INTERVAL APPROXIMATION($\mathbf{A}(t)$, $\mathbf{B}(t)$, T_p, $[t_0, t_f]$, $\mathbf{f}(t)$)
2: **subprocedure** FLOQUET MOMENT PROPAGATION($\mathbf{A}(t)$, $\mathbf{B}(t)$, T_p, $[t_0, t_f]$, $\mathbf{f}(t)$)
3: **end subprocedure** $\mu_S(t), \sigma_{SS}(t), \sigma_{\dot{S}\dot{S}}(t), \Sigma_{SS}(t_1, t_2)$
4: **subprocedure** EVD INTERVAL APPROXIMATION($\mu_S(t), \sigma_{SS}(t), \sigma_{\dot{S}\dot{S}}(t), \Sigma_{SS}(t_1, t_2)$, $[t_0, t_f]$, L)
5: **end subprocedure** $\hat{P}_f^c$
6: **end procedure**

Subprocedure 1: Floquet Moment propagation

Input: $\mathbf{A}(t)$, $\mathbf{B}(t)$, T_p, $[t_0, t_f]$, $\mathbf{f}(t)$
Output: $\mu_S(t), \sigma_{SS}(t), \sigma_{\dot{S}\dot{S}}(t), \Sigma_{SS}(t_1, t_2)$
7: **subprocedure** FLOQUET MOMENT PROPAGATION($\mathbf{A}(t)$, $\mathbf{B}(t)$, T_p, $[t_0, t_f]$, $\mathbf{f}(t)$)
8: Floquet Analysis: $\{\mathbf{R}(t), \mathbf{L}(t), \boldsymbol{\rho}\}$
9: Compute input's moments
10: Moment propagation: $\boldsymbol{\mu}_y(t), \boldsymbol{\Sigma}_{yy}(t_1, t_2)$ ▷ Eq. (19) and Eq. (21)
11: Response transformation: $\mu_S(t), \Sigma_{SS}(t_1, t_2)$ ▷ Eq. (20) and Eq. (22)
12: Differentiation and marginalization: $\sigma_{SS}(t)$ and $\sigma_{\dot{S}\dot{S}}(t)$
13: **end subprocedure**

Subprocedure 2: EVD Interval approximation

Input: $\mu_S(t), \sigma_{SS}(t), \sigma_{\dot{S}\dot{S}}(t), \Sigma_{SS}(t_1, t_2)$
Output: $\hat{P}_f^c$
14: **procedure** EVD INTERVAL APPROXIMATION($\mu_S(t), \sigma_{SS}(t), \sigma_{\dot{S}\dot{S}}(t), \Sigma_{SS}(t_1, t_2)$, $[t_0, t_f]$, L)
15: Initialize level zeroth: $I^T = [t_0, t_f]$
16: Compute the temporal mean of $\mu_S(t)$: $\xi = \frac{1}{t_f - t_0}\int_{t_0}^{t_f} \mu_S(t)\,\mathrm{d}t$
17: Form level one, $I^{(1)} = \bigcup_k I_k^{(1)}$, with each $I_i^{(1)} = [t_{0,i}, T_i]$;$\mu_S(t_{0,i}) - \xi = 0$, $\mu_S(T_i) - \xi = 0$ and $\mu_S(t) > \xi, \forall t \in I_i^{(1)}$
18: For each $I_k^{(1)}$, find: $\mu_S^{\max_i} = \max[\mu_{SS}(t)]$ and $(t^*, \sigma_{SS}^{\max_i}) = \max_t[\sigma_{SS}(t)], t \in I_k^{(1)}$, $\sigma_{\dot{S}\dot{S}}^i = \sigma_{\dot{S}\dot{S}}(t^*)$
19: Find β from Covariance β–analysis
20: Form level two $I^{(2)} = \bigcup_k I_k^{(2)}$ ▷ Eq. (26) and β
21: Compute each Δt_k from $I_k^{(2)}$
22: For each $I_k^{(1)}$, approximate $\hat{\lambda}_{S_k}^+(L)$ ▷ Eq. (17) and step 18
23: Compute the total EVD ▷ Eq. (24) and step 22
24: Compute $\hat{P}_f^c$ ▷ Eq. (23)
25: **end procedure**

Covariance β–analysis

Input: $\Sigma_{SS}(t_1, t_2)$, t^* from $I_k^{(1)}$
Output: β
26: **procedure** COVARIANCE β–ANALYSIS($\Sigma_{SS}(t_1, t_2)$, t^*)
27: Initialize $\beta \leftarrow \beta_0$
28: Compute $Z(\beta_0)$ ▷ Eq. (27) and Eq. (28)
29: $\beta \leftarrow \beta_0 + \epsilon$
30: **while** $Z(\beta) > Z(\beta_0)$ **do**
31: $\beta_0 \leftarrow \beta$
32: $\beta \leftarrow \beta_0 + \epsilon$
33: Compute $Z(\beta)$
34: **end while**
35: $\beta \leftarrow \beta_0$
36: **end procedure**

Fig. 3. Summary of algorithm implementation.

5. Numerical Application: Simplified Rotor-Blade Model under Gaussian and non-Gaussian non-Stationary Load

In this section, we introduce the necessary elements to test the proposed method. The deterministic LTP system is presented, and the physical meaning of the modelled quantities is established. The results from Floquet analysis are synthesized for the corresponding system. Two nonstationary stochastic loads are considered, and their description is provided. One load process, denoted Case A, is Gaussian in distribution; Case B is non-Gaussian, resulting from a monomial transformation of a Gaussian antecedent. Finally, the LSF under analysis is established and linked to its engineering interpretation in the domain of wind or tidal turbine design.

5.1. System description

The system describes a scale turbine undergoing planar motion confined to the plane of rotation; it is composed of one disc mounted on a rotor, and two blades attached to the disc radially with cantilever boundary conditions. The motion of the system is parametrized by the translation of the disc in the plane: x_1, x_2; and two modal variables represent the in-plane transverse vibration of each blade x_3, x_4 and x_5, x_6, respectively. The physical parameters of the rotor component are summarized in Table 2.

An Euler-Bernoulli beam model has been used for the blades. Kinematic discretization (Rayleigh-Ritz) in combination with the Assumed Modes method has been utilized to discretize the continuum. The Assumed Modes correspond to a polynomial approximation of the modes of the associated rotating beam problem. The parameters of this beam are provided in Table 3.

Table 3. Physical and mechanical properties of the blade component in the rotor-blade application.

Parameter	Values	Parameter	Values
Blade mass ($A\rho L_B$)	379.75 [kg]	Density (ρ)	7,750.0 [kg.m^{-3}]
Blade length (L_B)	5.0000 [m]	Modal damping (D_1, D_2)	2.00000; 5.00000
Young's modulus (E)	1.9600 × 10^{9} [Pa]	Cross-section's inertia (I)	3.835 × 10^{-7} [m^4]
Cross-sectional area (A)	9.8000 × 10^{-3} [m^2]	Angular Velocity (Ω)	$2\pi/5$ [rad.s^{-1}]

The state space representation of this system has 12 DOF, resulting in an LTP ODE system with as many equations. It can further be added that the blades have a constant, elliptical cross-section and the material under consideration is an iron-chromium-nickel-copper alloy, following reference [46].

From the mechanical model of the blades, it can be established that the Root Bending Moment (RBM) has the following expression:

$$M_{RBM}(t) = EI(\varphi_1(0)x_3(t) + \varphi_2(0)x_4(t)), \tag{30}$$

where φ_1 and φ_2 are the second derivatives of the mode shapes with respect to the spatial dimension, obtained from the kinematic discretization procedure. We take as critical value the RBM equal to 23 × 10³ [N.m].

5.2. Stochastic load and limit state function

Two input stochastic loads have been considered for the application, defining cases A and B. In both cases, the load process contains stationary and nonstationary components, consistent with the physical context of the problem: the action over the base is stationary, while the load on the blades is nonstationary by virtue of the relative angular velocity between the blades and the field generating the loads. The loads are generated by applying a monomial transformation and temporal modulation over an underlying Gaussian Stationary process $\mathbf{X}_G(t)$.

The underlying Gaussian Stationary process $\mathbf{X}_G(t)$ has the following mean function $\mu_{\mathbf{X}_G}$ and variance functions $\sigma^A_{\mathbf{X}_G\mathbf{X}_G}, \sigma^B_{\mathbf{X}_G\mathbf{X}_G}$:

$$\mu_{\mathbf{X}_G} = \begin{bmatrix} 0 \\ 0 \\ 0 \end{bmatrix}; \quad \sigma^A_{\mathbf{X}_G\mathbf{X}_G} = \begin{bmatrix} 1 \\ 250 \\ 250 \end{bmatrix}; \quad \sigma^B_{\mathbf{X}_G\mathbf{X}_G} = \begin{bmatrix} 1 \\ 50 \\ 50 \end{bmatrix}. \tag{31}$$

A uniform Power Spectral Density (PSD) has been used in both cases, with a frequency range: $f_{min} = 0.1[\mathrm{Hz}], f_{max} = 0.4[\mathrm{Hz}]$. The processes are simulated on the interval $t = [0, 16s]$, with $N_s = 1 \times 10^5$ samples.

The transformations applied to the underlying Gaussian in each case are given by the following expressions:

$$\mathbf{f}^A(t) = \begin{bmatrix} 100(X_{G,1}(t)+1) \\ X_{G,1}(t)+1 \\ (X_{G,2}(t)+250)\cos[\Omega t] \\ (X_{G,3}(t)+250)\cos[\Omega t] \\ -(X_{G,2}(t)+250)\cos[\Omega t] \\ -(X_{G,3}(t)+250)\cos[\Omega t] \end{bmatrix}; \quad \mathbf{f}^B(t) = \begin{bmatrix} 100(X_{G,1}(t)|X_{G,1}(t)|+1) \\ X_{G,1}(t)|X_{G,1}(t)|+1 \\ (X_{G,2}(t)|X_{G,2}(t)|+250)\cos[\Omega t] \\ (X_{G,3}(t)|X_{G,3}(t)|+250)\cos[\Omega t] \\ -(X_{G,2}(t)|X_{G,2}(t)|+250)\cos[\Omega t] \\ -(X_{G,3}(t)|X_{G,3}(t)|+250)\cos[\Omega t] \end{bmatrix} \tag{32}$$

In these expressions, Ω is the angular velocity parametrizing the rotation of the LTP system. The load process A is Gaussian in distribution, whereas the transformation generating process B ensures that Case B is non-Gaussian in distribution.

The LSF of interest has been selected as the RBM of blade 1:

$$G(t) = L - EI(\varphi_1(0)x_3(t) + \varphi_2(0)x_4(t)). \tag{33}$$

As previously stated, this level of RBM corresponds to the yield stress at the critical fiber of the section.

5.3. MCS benchmark

To establish the efficacy and correctness of the proposed method, a Monte-Carlo-based simulation strategy has been selected, given its generality and conceptual simplicity. This subsection provides the technical aspects of this benchmark.

1. The first step is the sampling of the input stochastic process $\mathbf{f}(t)$. A spectral representation method combined with process transformation techniques yields a load ensemble $\mathbf{f}^{(k)}(t_i)$ with $i = [1, \dots, n_t]$, with n_t discrete instants for $k = [1, \dots, n_s]$ samples. For the selected processes, $n_t = 70$ instants and $n_s = 10^5$ samples have been adopted based on stochastic convergence and underlying spectral properties.
2. The second step is the setup of an Initial Value Problem (IVP) with suitable integration tolerances for the resolution step through some numerical ODE solver. In this case, the initial conditions are set in such a way that the transient components of the solution are reduced, thus reaching the steady regime in a short integration time. The integration method is a variable order Adams-Bashforth-Moulton method, with a relative tolerance of 10^{-6} and absolute tolerance of 10^{-8}, the implementation is MATLAB's ODE113. The integration time is $T = [0, 3T_p]$, and the solution is interpolated on a uniform time grid of n = 5 × 10³ points.
3. The third step is the proper integration of the IVP for each realization, which is done in a parallel setup of 12 workers. This yields an ensemble $\mathbf{y}^{(k)}(t_j)$, $j = [1, \dots, 5 \times 10^3]$ of k solutions.
4. The fourth step is the transformation of the general solution variables for each realization into the selected limit-state response variable. From $G(t) = L - S(t)$, there is a suitable transformation matrix $\mathbf{C}$, such that $S^{(k)}(t_j) = \mathbf{C}\mathbf{y}^{(k)}(t_j)$ yielding the values of the LSF for each realization $G^{(k)}(t_j)$.
5. The final step is the computation of the estimators of the probability of failure in the total interval,

We introduce the following indicator function for the total probability of failure:

$$I^C(G^{(k)}(t)) = \begin{cases} 1, & \exists t \in T, \text{s.t. } G^{(k)}(t) \le 0 \\ 0, & \text{otherwise} \end{cases} \tag{34}$$

from which the probability of failure is calculated as the MC estimator:

$$P_f^C = \frac{1}{n_s} \sum_k I^C(G^{(k)}(t)). \tag{35}$$

As a measure of the statistical significance of these estimators, we employ the coefficient of variation:

$$\mathrm{C.o.V}\left[P_f^C\right] = \sqrt{\frac{1 - P_f^C}{n_s P_f^C}}. \tag{36}$$

6. Results and Discussion

6.1. Moment propagation and interval analysis of the response

The mean and variance of the response S(*t*) and its derivative are presented in Figs. 4 and 5 for each respective case. Interval approximation has been applied with four intervals of interest, with the parameters:

$$\beta_A = 0.99667 \quad \beta_B = 0.98888, \tag{37}$$

this selection has been made based on the shape of the variance function near its local maximum.

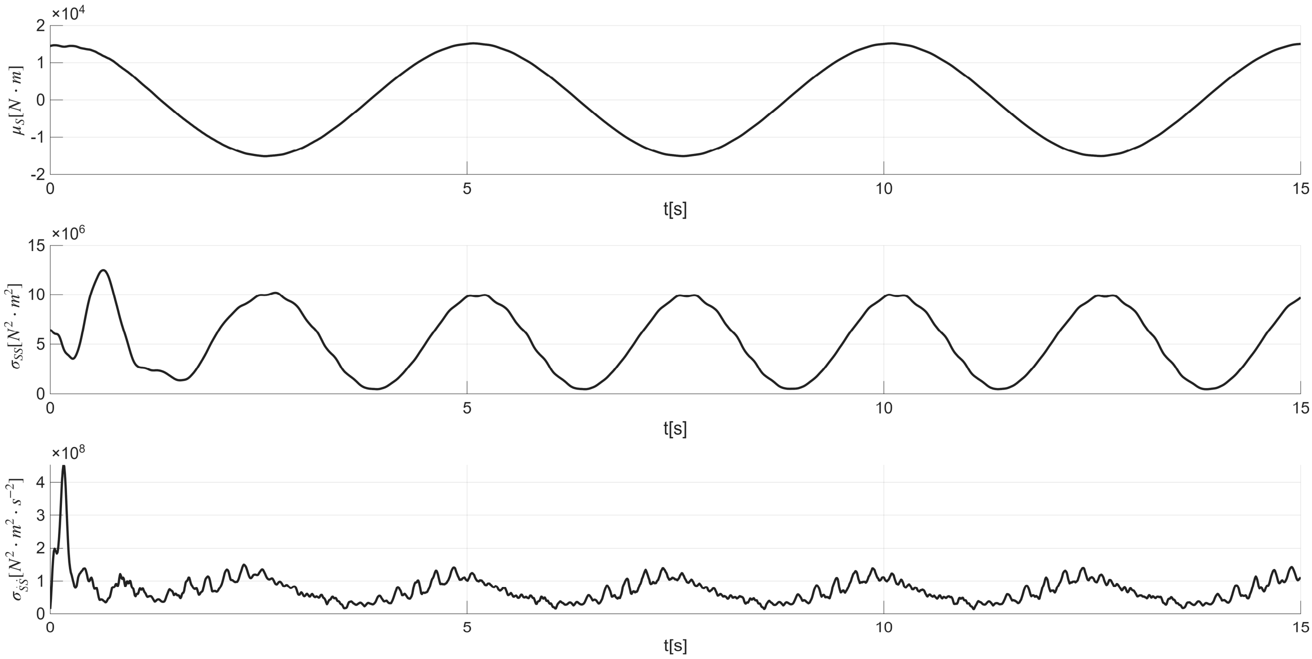

Fig. 4. Moments of the response in case A, from the Floquet convolution step.

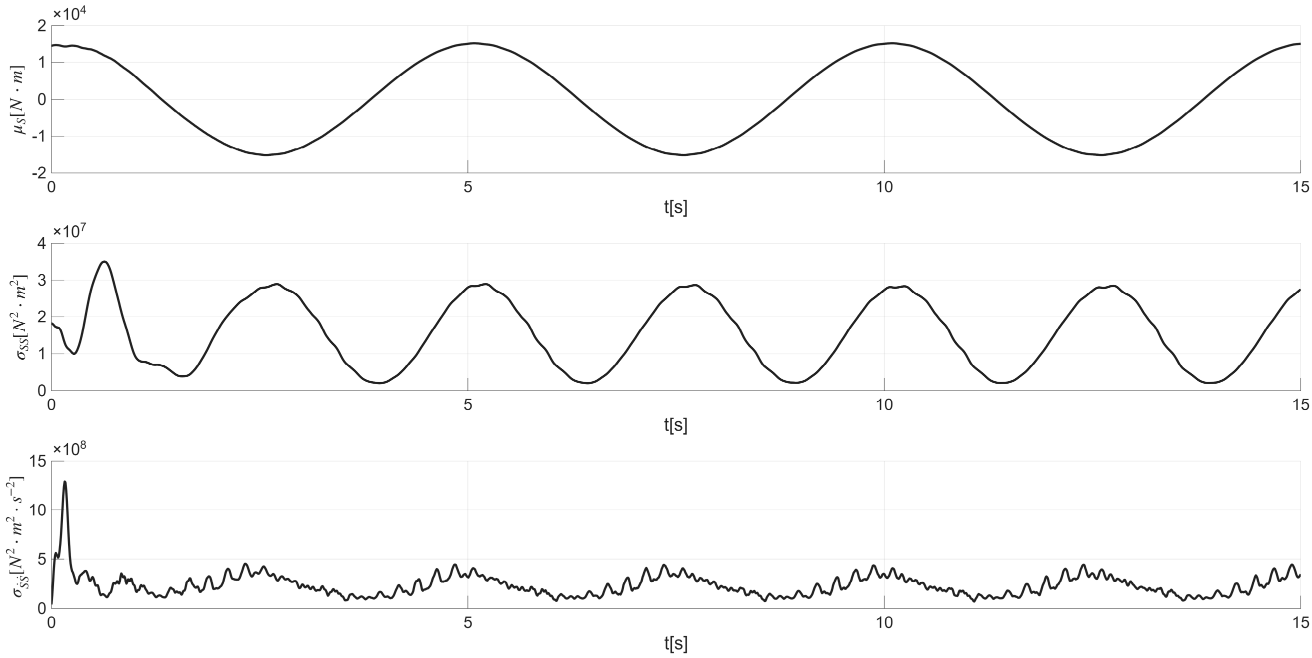

Fig. 5. Moments of the response in case B, from the Floquet convolution step.

Table 4. Equivalent intervals and moments, Case A (left) and B (right).

$I_i^{(2)}$	$\mu_S^{Max,i}$	$\sigma_{SS}^{Max,i}$	$\sigma_{\dot{S}\dot{S}}^{i}$	$I_i^{(2)}$	$\mu_S^{Max,i}$	$\sigma_{SS}^{Max,i}$	$\sigma_{\dot{S}\dot{S}}^{i}$
$[0.619, 0.654]$	1.46×10^{4}	1.25×10^{7}	4.00×10^{7}	$[0.603, 0.665]$	1.46×10^{4}	3.49×10^{7}	1.35×10^{8}
$[5.182, 5.236]$	1.51×10^{4}	9.95×10^{6}	8.97×10^{7}	$[5.145, 5.256]$	1.51×10^{4}	2.89×10^{7}	2.91×10^{8}
$[10.044, 10.090]$	1.51×10^{4}	9.97×10^{6}	1.07×10^{8}	$[10.050, 10.285]$	1.51×10^{4}	2.83×10^{7}	2.89×10^{8}
$[14.995, 15.000]$	1.49×10^{4}	9.68×10^{6}	1.11×10^{8}	$[14.983, 15.000]$	1.49×10^{4}	2.74×10^{7}	3.49×10^{8}

Table 5. Comparison of the proposed method with MCS, probability of failure over the entire interval [0, $3T_p$].

	P_f^C	C.o.V, P_f^C	$\hat{P}_f^C$	Err (%)
Case A	2.93×10^{-3}	0.058	2.94×10^{-3}	1.59×10^{-5} (0.5%)
Case B	6.71×10^{-2}	0.012	6.73×10^{-2}	2.18×10^{-4} (0.42%)

Table 6. Comparison of the proposed method with MCS, computation time.

Computation time [s]	MCS (parallel)	Proposed method
Case A	31,323	471
Case B	32,200	364

We observe that the peaks in variance are steeper for Case B, and the overall value of the variance for the associated derivative process is substantially larger, too. The mean function of the response in both cases is nearly identical, so we can informally express that Case B is more "variance-dominated" than Case A, although not to the degree of making Case B inadmissible for our approximation scheme.

The associated equivalence intervals and the value of moments are grouped in Table 4. Even though we have selected a uniform β for each problem, our selected criterion adapts to the form of the covariance function to produce appropriate subintervals for our final approximation.

6.2. Probability of failure and computation time

The predicted probability of failure, P_f^C, of the system over the entire observation interval $[0, 3T_p]$ is compared for each case with the MCS benchmark. Taking the MCS result as correct, the errors are reported as $\text{Err} = [\hat{P}_f^C - P_f^C]$, where $\hat{P}_f^C$ is the estimation by the proposed method and P_f^C is the MCS benchmark. The Coefficient of variation for the MCS estimator is provided in each case. These results are summarized in Table 5.

In both cases, the method shows close proximity to the benchmark result, with errors below 1%. Both predictions by the proposed method slightly overestimate the probability of failure. This is consistent with our theoretical discussion at the end of Section 4, supported by the parametric analysis in Appendix B. The result in Case B shows that the strategy has successfully approximated a non-Gaussian, non-stationary response to a high degree.

The usefulness of the proposed method becomes more apparent when the computation time is considered, as shown in Table 6. The MCS implementation in this work leverages the independence of MCS realizations by introducing a parallel resolution strategy that substantially reduces the required computation time. The simulation was executed on a computer with a 12th Gen Intel(R) Core(TM) i7-12700H processor at 2.30 GHz and 16.0 GB RAM, using MATLAB R2023b. Accounting for overhead times in parallel communication transfer among working units, the 12 parallel processes resulted in an estimated tenfold computation speedup as compared to the required time in sequential MCS implementations. With all these considerations, the convolution moment propagation combined with the proposed interval decomposition method required a computation time in seconds, of the order of magnitude 10^2, less than 10 minutes on each case. On the other hand, the MCS approach required 10^4, slightly less than 9 hours with parallelization.

These results indicate that Floquet modal convolution methods combined with the proposed interval approximation are a feasible strategy for fast reliability estimation of stochastically-excited LTP structures, producing estimators that slightly overestimate the probability of failure, with a moderate error whose behavior is known a priori.

7. Conclusion

We have introduced a new model-specific time-dependent reliability analysis method for stochastically excited rotor-blade models. The method relies on three distinct elements. First, semi-analytical, efficient moment-propagation convolution formulas based on Floquet theory permit the quantification of response moments, resulting in substantial savings in computation time compared to the Monte Carlo approach. Second, a dedicated algorithm based on a hierarchy of time subintervals allows for the identification of critical time intervals with a high probability of crossing for the corresponding LSF. Third, an EVD-based reliability estimation technique permits the evaluation of failure probability; the approach is based on asymptotic results. Our proposed interval decomposition and covariance analysis criterion facilitate the passage from idealized asymptotic results to more realistic situations with finite thresholds. This last element also permits the use of Poisson-like EVD distributions for LSFs derived from the stochastic response of time-periodic systems, overcoming the limitations of a direct application of the Poisson hypothesis to this class of system response.

Unlike popular time-varying reliability methods in the literature, ours is designed to handle problems arising from stochastic dynamics, especially those arising from rotor-blade models. The method has proven effective for analyzing Gaussian and non-Gaussian, non-stationary inputs, thereby contributing to the adoption of more sophisticated probabilistic models in the reliability analysis of rotor-blade models. Similarly, compared with widely used surrogate-based techniques, we have shown that exploiting the problem-specific structure provided by the Floquet representation yields substantial computational savings with modest technical prerequisites. Given the method's precision, our results suggest this is a promising avenue to explore. In the same vein, our framework accounts for the effects of system periodicity on blade vibration response, an aspect often neglected in the analysis of bladed systems. In this sense, our results contribute to the integration of time-periodic characteristics in this type of problem.

The method has a limitation: it can analyze only systems described by or approximated by the Floquet representation.

Additionally, the EVD approach to reliability limits its applicability: for LSFs that the EVD formulation cannot effectively handle, significant changes to our proposal would be required. Despite these limitations, our method is still applicable to a broad range of problems, including renewable energy, propulsion, and other industrial applications.

Author Contributions

O.S. Jimenez planned the scheme, developed the mathematical model, conducted the numerical experiments, and produced the first draft. E. Pagnacco initiated the project, suggested the experiments, contributed to the development of the mathematical model and its explanation, and revised the first draft. Y. Aoues examined the theory validation, analyzed empirical results, and revised the first draft. The manuscript was written through the contribution of all authors. All authors discussed the result, reviewed, and approved the final version of the manuscript.

Acknowledgments

The first author would like to thank Prof. Éric Jacquelin for his encouraging and edifying comments on the early stages of the idea behind this article. His remarks were a motivating force behind the pursuit of this research project.

Conflict of Interest

The authors declared no potential conflicts of interest concerning the research, authorship, and publication of this article.

Funding

The authors received no financial support for the research, authorship, and publication of this article.

Data Availability Statements

The datasets generated during the current study are available from the corresponding author on reasonable request.

Nomenclature

Symbol	Description	Symbol	Description
$\mathbf{A}(t),\mathbf{B}(t)$	State space system matrices	$\mathbf{q},\dot{\mathbf{q}}$	Floquet generalized variables and their time derivative
$\mathbf{C}$	Observation matrix	$\mathbf{R}(t)$	Matrix of Right Periodic Eigenvectors
$\mathrm{E}[\bullet]$	Mathematical expectation operator	$S(t)$	Limit state response
$\mathbf{f}(t)$	Physical load [N]	S_M	Extreme value of S(t)
$G(t)$	Limit state function	T_p	System's period [s]
$\mathbf{G}_t(t)$	Matrix of damping and gyroscopic coefficients	T	Final time [s]
$\mathbf{h}(t)$	Impulse response matrix	$\mathbf{x},\dot{\mathbf{x}},\ddot{\mathbf{x}}$	Vector of physical variables and its time derivatives
$I^T,I^{(1)},I^{(2)}$	Time interval hierarchy of levels zeroth, one, and two	$\mathbf{y},\dot{\mathbf{y}}$	Vector of state variables and its time derivative
$\mathbf{K}_t$	Stiffness matrix	β	Similarity parameter
L	Limit state available resistance [N.m]	$\lambda_S^+(L)$	Mean Number of crossings of S(t) over L
$\mathbf{L}(t)$	Matrix of Left Periodic Eigenvectors	$\mu_S(t)$	Mean function of process S(t) [N.m]
$\mathbf{M}(t)$	Mass-inertia matrix	$\nu_S^+(t)$	Crossing rate of S(t)
$M_{RBM}(t)$	Root Bending Moment [N.m]	$\boldsymbol{\rho}$	Matrix of Characteristic Exponents
$N(L,0,T)$	Number of crossings over L on the interval [0, T]	σ_{SS},Σ_{SS}	Variance function and Covariance matrix function of process S(t) [$N^2.m^2$]
$\mathbb{P}[\bullet]$	Probability operator	τ	Integration dummy variable
P_f^C	Total or cumulative probability of failure	φ_1,φ_2	Blade mode shape derivatives

References

[1] Carnegie, W., Vibrations of rotating cantilever blading: Theoretical approaches to the frequency problem based on energy methods, *Journal of Mechanical Engineering Science*, 1(3), 1959, 235–240.
[2] Khulief, Y.A., Laejoon, Y., Lead-lag vibrational frequencies of a rotating beam with end mass, *Computers & Structures*, 29(6), 1988, 1075–1085.
[3] Leung, T. C., Fung, A. Y. T., Spinning finite elements, *Journal of Sound and Vibration*, 125(3), 1988, 523–537.
[4] Ganguli, R., *Finite Element Analysis of Rotating Beams: Physics Based Interpolation*, Springer, Singapore, 2017.
[5] Christensen, R. H., *Active Vibration Control of Rotor-blade Systems: Theory and Experiment*, PhD Thesis, Department of Mechanical Engineering, Technical University of Denmark, Kgs Lyngby, 2004.
[6] Bottasso, C. L, Cacciola, S., Model-independent periodic stability analysis of wind turbines, *Wind Energy*, 18(5), 2015, 865–887.
[7] Hansen, M. H., Modal dynamics of structures with bladed isotropic rotors and its complexity for two-bladed rotors, *Wind Energy Science*, 1(2), 2016, 271–296.
[8] Firouzi, N., Lenci, S., Amabili, M., Rabczuk, T., Nonlinear free vibrations of Timoshenko–Ehrenfest beams using finite element analysis and direct scheme, *Nonlinear Dynamics*, 112(9), 2024, 7199-7213.
[9] Firouzi, N., Dohnal, F., Dynamic stability of the Mindlin-Reissner plate using a time-modulated axial force, *Mechanics Based Design of Structures and Machines*, 53(1), 2025, 446-463.

[10] Xu, J., Gasch, R., Modale Behandlung linearer periodisch zeitvarianter Bewegungsgleichungen, *Archive of Applied Mechanics*, 65, 1995,178-193.
[11] Floquet, G., Sur les équations différentielles linéaires à coefficients périodiques, *Annales Scientifiques de l'École Normale Supérieure*, 12, 1883, 47–88.
[12] Kelley, W. G., Peterson, A. C., *The Theory of Differential Equations*, Springer, New York, 2010.
[13] Ma, H., Lu, Y., Wu, Z., Tai, X., Li, H., Wen, B., A new dynamic model of rotor–blade systems, *Journal of Sound and Vibration*, 357, 2015, 168-194.
[14] Li, B., Ma, H., Yu, X., Zeng, J., Guo, X., Wen, B., Nonlinear vibration and dynamic stability analysis of rotor-blade system with nonlinear supports, *Archive of Applied Mechanics*, 89(7), 2019, 1375-1402.
[15] Wu, J., Rezgui, D., Titurus, B., Dynamics of nonlinear beam-propeller system with different numbers of blades, *Nonlinear Dynamics*, 112(2), 2024, 833-863.
[16] Forghani, S. M., Ritto, T. G., Stochastic analysis on the stability of the solutions of wind turbine blade vibrations applying the Floquet theory, *11th International Conference on Engineering Vibration*, Ljubljana, Slovenia, 2015.
[17] Kumar, R., Ali, S. F., Gupta, S., Stochastic reduced order modelling and analysis of rotating bladed discs, *Proceedings of the Royal Society A*, 478(2260), 2022, 20210833.
[18] Bae, H., Boyd, I. M., Carper, E. B., Brown, J., Accelerated multifidelity emulator modeling for probabilistic rotor response study, *Journal of Engineering for Gas Turbines and Power*, 141(12), 2019, 121019.
[19] Sánchez Jiménez, O., *On the stochastic response of rotor-blade models with Floquet modal theory: applications to time-dependent reliability of tidal turbine blades*, PhD Thesis, Laboratoire de Mécanique de Normandie, Normandie Université, Saint-Étienne-du-Rouvray, 2023.
[20] Prelewicz, D. A., Response of linear periodically time varying systems to random excitation, *AIAA Journal*, 10(8), 1972, 1124–1125.
[21] Spires, J. M., Sinha, S. C., On the response of linear time-periodic systems subjected to deterministic and stochastic excitations, *Journal of Vibration and Control*, 2(2), 1996, 219–249.
[22] Han, X., Sánchez Jiménez, O., Pagnacco, E., Response and EPSD of rotor-blade nonlinear system with non-stationary non-gaussian stochastic excitation via PGHW method, *Computers & Mathematics with Applications*, 142, 2023, 140–156.
[23] Rackwitz, R., Reliability analysis-a review and some perspectives, *Structural Safety*, 23(4), 2001, 365–395.
[24] Zhang, B., Wang, W., Wang, Y., Li, Y., Li, C-Q., A critical review on methods for time dependent structural reliability, *Sustainable and Resilient Infrastructure*, 9(2), 2023, 91–106.
[25] Sudret, B., *Uncertainty propagation and sensitivity analysis in mechanical models–contributions to structural reliability and stochastic spectral methods*, H. D. R. Thesis, Université Blaise Pascal, Clermont-Ferrand, France, 2007.
[26] Andrieu-Renaud, C., Sudret, B., Lemaire, M., The PHI2 method: a way to compute time-variant reliability, *Reliability Engineering & System Safety*, 84(1), 2004, 75–86.
[27] Sudret, B., Analytical derivation of the outcrossing rate in time-variant reliability problems, *Structure and Infrastructure Engineering*, 4(5), 2008, 353–362.
[28] Hu, Z., Du, X., Time-dependent reliability analysis with joint upcrossing rates, *Structural and Multidisciplinary Optimization*, 48(5), 2013, 893–907.
[29] Hu, Z., Du, X., Mixed efficient global optimization for time-dependent reliability analysis, *Journal of Mechanical Design*, 137(5), 2015, 051401.
[30] Gong, C., Frangopol, D. M., An efficient time-dependent reliability method, *Structural Safety*, 81, 2019, 101864.
[31] Echard, B., Gayton, N., Lemaire, M., AK-MCS: an active learning reliability method combining kriging and Monte Carlo simulation, *Structural Safety*, 33(2), 2011, 145–154.
[32] Hu, Z., Mahadevan, S., A single-loop kriging surrogate modeling for time-dependent reliability analysis, *Journal of Mechanical Design*, 138(6), 2016, 061406.
[33] Attukur Nandagopal, R., Narasimalu, S., Chai, G. B., Probabilistic structural reliability analysis of a horizontal axis tidal turbine blade by considering the moisture effects on the blade material, *Marine Systems & Ocean Technology*, 15(4), 2020, 253-269.
[34] Val, D. V., Chernin, L., Yurchenko, D. V., Reliability analysis of rotor blades of tidal stream turbines, *Reliability Engineering & System Safety*, 121, 2014, 26-33.
[35] Friswell, M. I., *Dynamics of rotating machines*, Cambridge University Press, New York, 2010.
[36] Genta, G., *Dynamics of rotating systems*, Springer, New York, 2005.
[37] Géradin, M., Rixen, D. J., *Mechanical vibrations theory and application to structural dynamics*, John Wiley & Sons, New York, 2014.
[38] Rice, S. O., Mathematical analysis of random noise, *The Bell System Technical Journal*, 23(3), 1944, 282–332.
[39] Rice, S. O., Mathematical analysis of random noise, *The Bell System Technical Journal*, 24(1), 1945, 46–156.
[40] Lindgren, G., Gaussian Integrals and Rice Series in Crossing Distributions—to Compute the Distribution of Maxima and Other Features of Gaussian Processes, *Statistical Science*, 34(1), 2019, 100-128.
[41] Hasofer, A. M., Petocz, P., *Extreme Response of the Linear Oscillator with Modulated Random Excitation, Statistical Extremes and Applications*, Springer, Netherlands, 1984, 503–512.
[42] Lutes, L. D., Sarkani, S., *Random vibrations: analysis of structural and mechanical systems*, Elsevier, Massachusetts, 2004.
[43] Suptille, M., *Caractérisation temporelle et spectrale de champs instationnaires non gaussiens: application aux hydroliennes en milieu marin*, Ph.D. Thesis, INSA de Rouen Normandie, Saint-Étienne-du-Rouvray, 2015.
[44] Ambetkar, V., Kuppa, R., Gupta, S., Multivariate Extreme Value Distributions for Vector of Non-stationary Gaussian Processes, *Procedia Engineering*, 144, 2016, 504–511.
[45] Konstant, D. G., Piterbarg, V. I., Extreme values of the cyclostationary Gaussian random process, *Journal of Applied Probability*, 30(1), 1993, 82–97.
[46] Clara, T., Falcão De Campos, J. A. C., Baltazar, J., Added mass effects on the natural frequencies of marine current turbine blades, *Proceedings of the 6th International Conference on Mechanics and Materials in Design*, Ponta Delgada, Azores, Portugal, 5524, 2014.

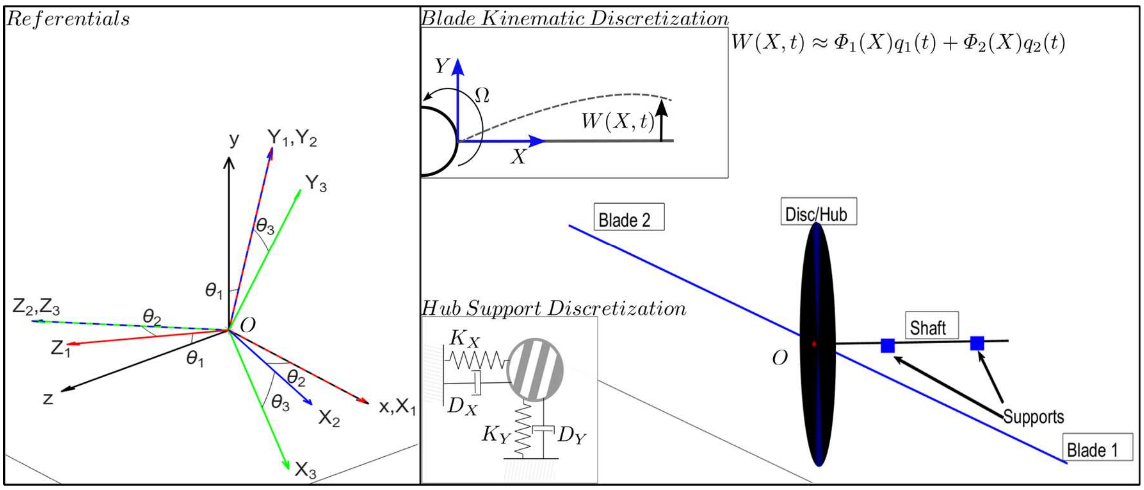

Fig. A1. Rotor-blade system diagrams with referentials (left) and main discretization aspects (right) for the modelling of the linear time-periodic dynamical system.

Appendix A: Dynamical Model of 6-DOF Rotor-Blade System

In this appendix, we provide additional information about our treatment of the system presented in Fig. 1. In Fig. A1, we present a diagram highlighting the main features of a rotor–blade model. First, a general 5–DOF rigid rotor on elastic foundations is presented, with the four traditional reference frames required to analyze its kinematics. The 5–DOF correspond to the three translations of the rotor solid, and two angular coordinates, with the third angular coordinate being prescribed by the constant rotational speed to which the body is subjected. We assume small angular motion, that is, the translation in the direction of the shaft's longitudinal axis is negligible. In such a case, the 5–DOF rotor model can be simplified to a 2–DOF planar motion rotor system, describing the dynamics of the system in Fig. 1.

Figure A1 provides the referential involved in the rotordynamics modelling of the system, the equivalent damping and stiffness parameters to represent the mast and supports, and the modal discretization of the blades. This treatment allows us to express the system in Fig. 1 as a linear time-periodic dynamical system by using the Euler-Lagrange formalism.

The system matrices have the following structure:

$$\mathbf{M}(t)=\begin{pmatrix} M+2A\rho L_B & 0 & -\psi_1\sin[\Omega t+\alpha_1] & -\psi_2\sin[\Omega t+\alpha_1] & -\psi_1\sin[\Omega t+\alpha_2] & -\psi_2\sin[\Omega t+\alpha_2] \\ 0 & M+2A\rho L_B & \psi_1\cos[\Omega t+\alpha_1] & \psi_2\cos[\Omega t+\alpha_1] & \psi_1\cos[\Omega t+\alpha_2] & \psi_2\cos[\Omega t+\alpha_2] \\ -\psi_1\sin[\Omega t+\alpha_1] & \psi_1\cos[\Omega t+\alpha_1] & \psi_{11} & \psi_{12} & 0 & 0 \\ -\psi_2\sin[\Omega t+\alpha_1] & \psi_2\cos[\Omega t+\alpha_1] & \psi_{12} & \psi_{22} & 0 & 0 \\ -\psi_1\sin[\Omega t+\alpha_2] & \psi_1\cos[\Omega t+\alpha_2] & 0 & 0 & \psi_{11} & \psi_{12} \\ -\psi_2\sin[\Omega t+\alpha_2] & \psi_2\cos[\Omega t+\alpha_2] & 0 & 0 & \psi_{12} & \psi_{22} \end{pmatrix} \tag{A.1}$$

$$\mathbf{G}_G(t)=\Omega\begin{pmatrix} 0 & 0 & -\psi_1\cos[\Omega t+\alpha_1] & -\psi_2\cos[\Omega t+\alpha_1] & -\psi_1\cos[\Omega t+\alpha_2] & -\psi_2\cos[\Omega t+\alpha_2] \\ 0 & 0 & -\psi_1\sin[\Omega t+\alpha_1] & -\psi_2\sin[\Omega t+\alpha_1] & -\psi_1\sin[\Omega t+\alpha_2] & -\psi_2\sin[\Omega t+\alpha_2] \\ \psi_1\cos[\Omega t+\alpha_1] & \psi_1\sin[\Omega t+\alpha_1] & 0 & 0 & 0 & 0 \\ \psi_2\cos[\Omega t+\alpha_1] & \psi_2\sin[\Omega t+\alpha_1] & 0 & 0 & 0 & 0 \\ \psi_1\cos[\Omega t+\alpha_2] & \psi_1\sin[\Omega t+\alpha_2] & 0 & 0 & 0 & 0 \\ \psi_2\cos[\Omega t+\alpha_2] & \psi_2\sin[\Omega t+\alpha_2] & 0 & 0 & 0 & 0 \end{pmatrix} \tag{A.2}$$

$$\mathbf{D}=\begin{pmatrix} D_X & 0 & 0 & 0 & 0 & 0 \\ 0 & D_Y & 0 & 0 & 0 & 0 \\ 0 & 0 & D_S\psi_{11} & D_S\psi_{12} & 0 & 0 \\ 0 & 0 & D_S\psi_{12} & D_S\psi_{22} & 0 & 0 \\ 0 & 0 & 0 & 0 & D_S\psi_{11} & D_S\psi_{12} \\ 0 & 0 & 0 & 0 & D_S\psi_{12} & D_S\psi_{22} \end{pmatrix} \tag{A.3}$$

$$\mathbf{K}_t=\begin{pmatrix} K_X & 0 & 0 & 0 & 0 & 0 \\ 0 & K_Y & 0 & 0 & 0 & 0 \\ 0 & 0 & K_{q_{11}q_{11}} & K_{q_{11}q_{12}} & 0 & 0 \\ 0 & 0 & K_{q_{12}q_{11}} & K_{q_{12}q_{12}} & 0 & 0 \\ 0 & 0 & 0 & 0 & K_{q_{21}q_{21}} & K_{q_{21}q_{22}} \\ 0 & 0 & 0 & 0 & K_{q_{21}q_{22}} & K_{q_{22}q_{22}} \end{pmatrix} \tag{A.4}$$

Here, $\mathbf{G}_t(t)=\mathbf{G}_G(t)+\mathbf{D}$. The coefficients can be computed by integrating the modal approximation of the beams and their derivatives:

$$\begin{aligned} \psi_i &= A\rho\int_0^{L_B}\Phi_{ii}(X)dX \\ \psi_{ij} &= A\rho\int_0^{L_B}\Phi_{ii}(X)\Phi_{jj}(X)dX. \end{aligned} \tag{A.5}$$

In the previous expressions Φ_{ii} is the modal shape approximation and X is the longitudinal dimension along the blade. The setting angle of each blade is fixed to $\alpha_1=0,\alpha_2=\pi$, respectively. For the stiffness matrix, we introduce:

$$\begin{gathered} \mathbf{K}_0=\begin{pmatrix}\psi_{11} & \psi_{12}\\ \psi_{21} & \psi_{22}\end{pmatrix},\quad \mathbf{K}_1=\begin{pmatrix}\int_0^{L_B}(\Phi_{11}')^2\,dX & \int_0^{L_B}\Phi_{11}'\Phi_{12}'dX\\ \int_0^{L_B}\Phi_{11}'\Phi_{12}'dX & \int_0^{L_B}(\Phi_{12}')^2\,dX\end{pmatrix},\quad \mathbf{K}_2=\begin{pmatrix}\int_0^{L_B}X(\Phi_{11}')^2\,dX & \int_0^{L_B}X\Phi_{11}'\Phi_{12}'dX\\ \int_0^{L_B}X\Phi_{11}'\Phi_{12}'dX & \int_0^{L_B}X(\Phi_{12}')^2\,dX\end{pmatrix} \\ \mathbf{K}_3=\begin{pmatrix}\int_0^{L_B}X^2(\Phi_{11}')^2\,dX & \int_0^{L_B}X^2\Phi_{11}'\Phi_{12}'dX\\ \int_0^{L_B}X^2\Phi_{11}'\Phi_{12}'dX & \int_0^{L_B}X^2(\Phi_{12}')^2\,dX\end{pmatrix},\quad \mathbf{K}_4=\begin{pmatrix}\int_0^{L_B}(\Phi_{11}'')^2\,dX & \int_0^{L_B}\Phi_{11}''\Phi_{12}''dX\\ \int_0^{L_B}\Phi_{11}''\Phi_{12}''dX & \int_0^{L_B}(\Phi_{12}'')^2\,dX\end{pmatrix} \end{gathered} \tag{A.6}$$

We next write:

$$\mathbf{K}_{q_{ii}q_{1i}}=\Omega^2\left(-\mathbf{K}_0+\kappa_1\mathbf{K}_1+\kappa_2\mathbf{K}_2+\kappa_3\mathbf{K}_3\right)+\kappa_4\mathbf{K}_4 \tag{A.7}$$

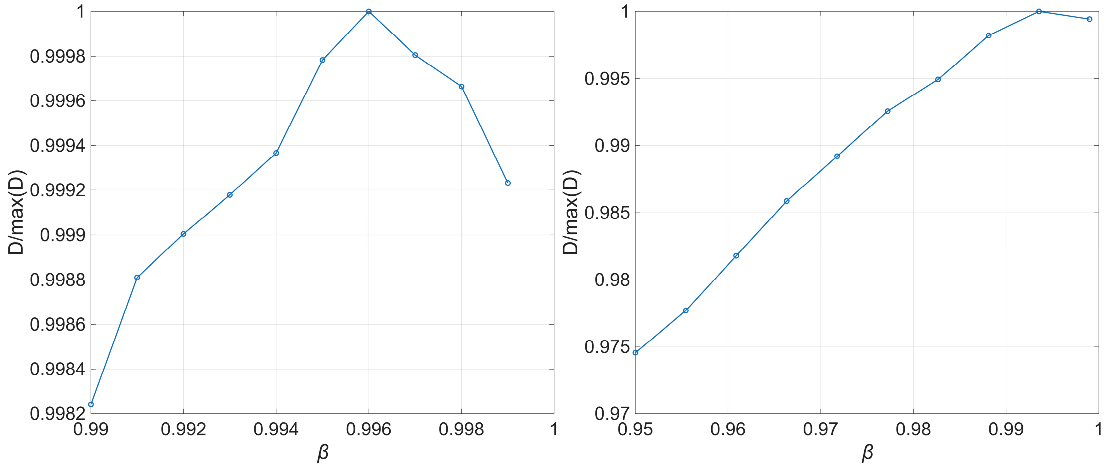

Fig. B1. Parametric analysis of β for the proposed selection criterion using the determinant of the discretized covariance function for the response process between peak variance instant and the end of the interval selected with the parameter: to the left, the analysis of Problem A, to the right, the analysis of Problem B; the determinant is normalized by its maximum observed value to facilitate visualization; the selected beta is right before the observed maximum on each plot.

With the following coefficients:

$$\begin{aligned} \kappa_1 &= AL_B\rho(L_B + 2r) \\ \kappa_2 &= -2rA\rho \\ \kappa_3 &= -A\rho \\ \kappa_4 &= EI. \end{aligned} \tag{A.8}$$

The structure of the state space matrices is the following:

$$\mathbf{A}(t) = \begin{pmatrix} \mathbf{0}_6 & \mathbf{I}_6 \\ -\mathbf{MK}_t & -\mathbf{M}^{-1}\mathbf{G}_t \end{pmatrix} \tag{A.9}$$

$$\mathbf{B}(t) = \begin{pmatrix} \mathbf{0}_6 \\ -\mathbf{M}^{-1} \end{pmatrix} \tag{A.10}$$

In these expressions, $\mathbf{0}_6$ is the null 6×6 matrix, and $\mathbf{I}_6$ is the identity 6×6 matrix. The observation matrix used can be written as $\mathbf{C} = c_j, j = 1,\ldots,12$ with:

$$c_j = \begin{cases} EI\varphi_1(0) & j = 3 \\ EI\varphi_2(0) & j = 4 \\ 0 & \text{otherwise.} \end{cases} \tag{A.11}$$

Appendix B: Analysis of the Parameter β

The similarity parameter β has a large impact on the results obtained in our approximation. It needs to be selected so that the final intervals are sufficiently close to the process at maximum variance, yet not so close that instants become indistinguishable and we lose coverage of important instants where crossings are still likely to occur. We present here a parametric study of β with respect to our selected criterion: the inflection point of the determinant of the discretized covariance function between the response at peak variance and at the end of the final interval. These results are synthesized in Fig. B1.

ORCID ID

Oscar Sanchez Jimenez https://orcid.org/0000-0002-5731-4794
Emmanuel Pagnacco https://orcid.org/0000-0001-5551-2511
Younes Aoues https://orcid.org/0000-0001-6543-8546

How to cite this article: Sanchez Jimenez O., Pagnacco E., Aoues Y. Time-Dependent Reliability Analysis of Rotor-Blade Systems with Floquet-Moment-EVD Interval Approximation, *J. Appl. Comput. Mech.*, 12(3), 2026, 1069-1083. https://doi.org/10.22055/jacm.2025.48746.5475